Ann. Phys. (Berlin) **525**, No. 1–2, 162–170 (2013) / DOI 10.1002/andp.201200269

annalen der physik

Original Paper

Secondary electron imaging of nanostructures using Extreme Ultra-Violet attosecond pulse trains and Infra-Red femtosecond pulses

*Erik Mårsell, Cord L. Arnold, Eleonora Lorek, Diego Guenot, Thomas Fordell, Miguel Miranda, Johan Mauritsson, Hongxing Xu, Anne L'Huillier, and Anders Mikkelsen**

Received 29 November 2012, revised 6 December 2012, accepted 6 December 2012
Published online 2 January 2013

Surface electron dynamics unfold at time and length scales down to attoseconds and nanometres, making direct imaging with extreme spatiotemporal resolution highly desirable. However, this has turned out to be a major challenge even with the advent of reliable attosecond light sources. In this paper, photoelectrons from Ag nanowires and nanoparticles excited by extreme ultraviolet (XUV) attosecond pulse trains and infrared femtosecond pulses using a PhotoEmission Electron Microscope (PEEM) are imaged. In addition, the samples were investigated using Scanning Electron Microscopy (SEM) and synchrotron based X-ray photoelectron spectroscopy (XPS). To achieve contrast between the nanostructures and the substrate in the XUV images, three different substrate materials were investigated: Cr, ITO and Au. While plasmonic field enhancement can be observed on all three substrates, only on Au substrates do the Ag nanowires appear significantly brighter than the substrate in XUV-PEEM imaging. 3-photon photoemission imaging of plasmonic hot-spots was performed where the autocorrelation trace is observed in the interference signal between two femtosecond Infra-Red (IR) beams with sub-cycle precision. Finally, using Monte Carlo simulations, it is shown how the secondary electrons imaged in the XUV PEEM can potentially reveal information on the attosecond time scale from the near surface region of the nanostructures.

1 Introduction

Imaging and spectroscopy of nanostructured materials using laser generated extreme ultraviolet (XUV) pulses going down to the attosecond timescale has attracted much attention in recent years [1]. At these very fast timescales collective electron motion becomes central, and nanoplasmonics is a good example of an important research area which can benefit strongly from time dependent imaging methods [1]. Nanoplasmonic materials have a broad range of applications [2–5] and many fundamental questions concerning their spatio-temporal behaviour remain unresolved [6–8].

The Photoemission Electron Microscope (PEEM) allows for excellent combined spatial and temporal resolution, as the incoming light used for excitation can provide high time resolution, while imaging the outgoing photoelectrons can be done with high spatial resolution. In nanoplasmonics, PEEM has mostly been used to image photoelectrons generated via two-photon photoemission processes, which visualize the electric field enhancement close to the surface. Combined with the PEEM's ability to also image nanoscale surface geometrical and chemical properties this turns out to be a very powerful way of studying plasmonics [9–16]. The interaction between an oscillating electric field and a metal surface is known to be rather complex, especially in the region close to the surface [17], which has also been explored by photoemission above the work function threshold coupled with theoretical calculations [18, 19].

Recently Stockman *et al.* [20] suggested to investigate plasmonic near-fields with PEEM and attosecond light pulses, thus achieving simultaneously high temporal and spatial resolution. They proposed the use of time-of-flight PEEM, in order to image the primary electrons with energy resolution, to directly measure the exterior nanoplasmonic field by nanometre-resolved attosecond

* Corresponding author: E-mail: anders.mikkelsen@sljus.lu.se
Department of Physics, Lund University, Box 118, 221 00 Lund, Sweden

streaking spectroscopy in the regime of instantaneous acceleration. One general challenge with this and other ultra-fast imaging schemes involving electrons is that the total number of photoemitted electrons must be strongly limited to avoid space charge problems. To resolve this, the peak intensities of each pulse has to be reduced, which can then increase acquisition times to unsustainable levels due to the low repetition rate of the light source involved. This might be resolved by future MHz repetition rate attosecond laser systems, but for present day kHz sources the experiments pose quite a challenge [21, 22]. Many other advanced light sources, such as free electron lasers, potentially suffer from similar space charge problems [23]. In addition to the primary electrons also secondary electrons (SEs) are released in attosecond XUV experiments. These derive from the primary electrons colliding with other electrons in the material thus starting an electron cascade. The intensity of the SEs typically makes out more than 90% of the emitted electrons in any experiment involving either electron or high-energy photon induced electron emission. As a result, the role of these SEs in the exploration of attosecond dynamics should be investigated and their use would be desirable as they are in fact very well suited for imaging also of a variety of electronic properties of samples. The SEs have for example been shown to give strong contrast in PEEM imaging for a number of electronic, chemical and magnetic effects [24–27].

In this paper, we present experimental and theoretical studies towards the realization of attosecond IR pump/XUV probe measurements under realistic conditions. Ag nanowires and nanoparticles, widely used in nanoplasmonics [28–30], were imaged by PEEM using XUV attosecond pulse trains. To optimize contrast between the nanostructures and the substrate in the XUV images, three different substrate materials were investigated: Cr, ITO and Au. The same structures were imaged using femtosecond IR pulses. We observed polarization-dependent plasmonic hot spots, and we performed an autocorrelation measurement of these structures. Finally, we present theoretical Monte Carlo simulations of the SE cascade following excitation by a single attosecond pulse (SAP), in conditions close to our experiment. These experimental and theoretical studies show that photoemission electron microscopy of surfaces using single attosecond pulses combined with a short IR laser pulse has the potential to reveal ultrashort surface/plasmon dynamics. Even SEs emitted after the primary excitation and imaged by the PEEM escape fast enough to provide information on the attosecond time scale.

2 Imaging nanostructures using XUV attosecond pulse trains (APTs)

We experimentally investigate the feasibility of SE imaging using an attosecond setup particularly suited for time-resolved PEEM measurements. This setup represents an advanced and relevant system which combines attosecond pulse trains (APTs) with IR pulses. As test objects, we used Ag nanowires and nanoparticles, which have been used in a number of previous plasmonic studies [28, 29]. The samples used in the experiments were prepared by depositing Ag nanostructures from colloidal solutions onto different substrates. We used nanowires, near-spherical nanoparticles, nanorice and nanocubes all dispersed in ethanol solution [31–33]. A drop of the solution was placed onto a substrate which was blow-dried after 30 seconds. The sample was then cleaned in acetone in an ultrasonic bath for 5 min. Three substrates were used: 50 nm thick Au film on Si, 50 nm Cr film on Si and 150 nm ITO film on borosilicate glass. Specific structures investigated in the PEEM could be recognized and studied in SEM. We also recorded XPS spectra at beamline I311 at the MAX-II synchrotron of the different samples, to monitor overall surface chemical composition and energy distribution of photoemitted electrons over a wide energy range.

The experimental atto-PEEM setup is schematized in Fig. 1(a). The Ti:Sapphire-based chirped pulse amplification laser system delivers ultrashort IR pulses of 35 fs (FWHM) duration, centered at 800 nm, with a pulse energy of ∼3 mJ, at a repetition rate of 1 kHz [34, 35]. The laser pulse is sent into an actively stabilized Mach-Zehnder interferometer [35], where in one arm attosecond XUV pulse trains, with one pulse per half-cycle, are generated via high-order harmonic generation (HHG) in a pulsed Ar gas cell. The XUV radiation is subsequently separated from the IR by passing through a 200 nm thick Al filter, and then propagates through a hole in a mirror which recombines the XUV with the IR from the second interferometer arm. A piezo delay stage allows for precise sub-cycle temporal delay between the attosecond pulses and the IR laser pulses. The XUV and IR pulses propagate collinearly and are focused by a toroidal mirror into the sensitive region of a magnetic bottle electron spectrometer (MBES), which is routinely used for characterization of the attosecond pulse trains via the RABBITT technique [36–38]. After the MBES, a PEEM (Focus GmbH) is placed in the beamline. The spatial resolution that can be achieved with APTs and Hg lamp in this setup is of the order of 200 nm and 50 nm, respectively. The XUV radiation is defocused at the position of the PEEM in order to avoid

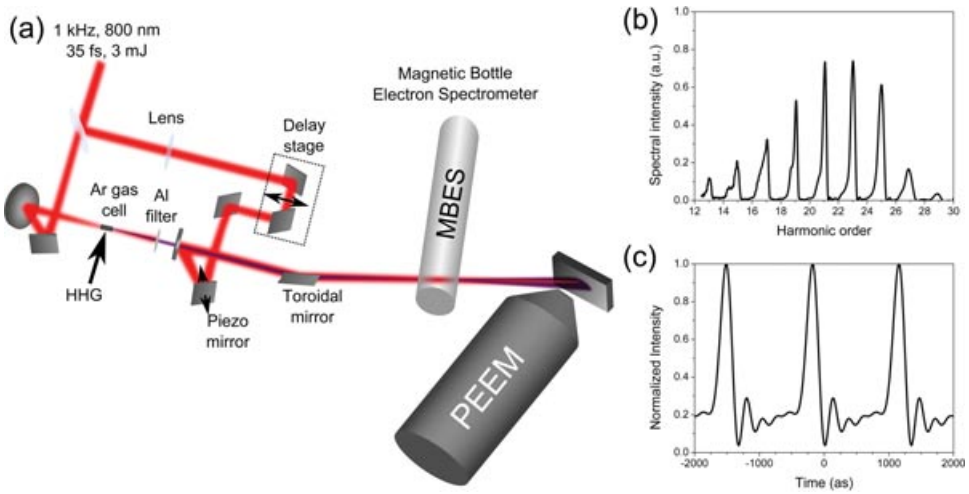

Figure 1 (online color at: www.ann-phys.org) (a) Sketch of the experimental setup for atto-PEEM measurements, consisting of an attosecond pump-probe interferometer, followed by an MBES (for attosecond pulse characterization), and the PEEM. (b) Typical spectrum of the XUV radiation. (c) Time-domain reconstruction of an attosecond pulse train.

too high XUV intensity. However, in order to get high enough IR intensities, we move its focus closer to the target by adding a lens in the IR arm of the interferometer. The samples located in the PEEM are illuminated at 65° angle to the normal and both beams are s-polarized unless otherwise specified. Photoelectrons emitted from the sample by plasmon-enhanced 3-photon photoemission with the IR ultrashort pulses or 1-photon photoemission from the XUV attosecond pulse trains are accelerated by a strong electric field (typically 10–15 kV over a distance of 1.8 mm) and projected by a set of electrostatic lenses onto an MCP/YAG imaging unit.

The short pulse duration of the attosecond pulses (200 as in the present case) leads to very broadband radiation, and our pulses have a bandwidth that is ∼12 eV (FWHM) centered around 30 eV. The use of a pulse train instead of SAPs leads to an excitation by discrete harmonic peaks as shown in Fig. 1(b-c). Due to the very large bandwidth, obtaining a good contrast with this type of radiation, without energy filtering, is a challenge. We experimentally investigated the contrast that can be achieved by detecting all electrons emitted by broadband APTs. The imaging contrast should be similar for APTs compared to SAPs in the same spectral region (we indeed see no deterioration in image quality by using XUV radiation produced by significantly shorter 7 fs IR pulses), making APT imaging an important step towards imaging with ultrahigh spatiotemporal resolution.

Figure 2 shows XUV-PEEM images of Ag nanowires and nanoparticles on different substrates: ITO, Cr, and Au. Experiments have also been performed using semiconductor substrates such as Si or InAs, but the lower conductivity of these substrates led to severe problems with charging of the samples. The contrast obtained with PEEM imaging depends on a number of different aspects, such as topography, work function, and ionization cross-section. The ITO, Cr, and Au substrates give very different contrast, as indicated by the profiles across the nanowires in Fig. 2, where we have selected the regions that give the highest contrast in each image. On the ITO substrate, most nanowires appear black (i.e., they show a photoemission yield significantly lower than that from the substrate). There is also no clear orientation dependence. This suggests an electronic structure contrast mechanism that is sensitive to the surface of the wire, with the vast majority of structures emitting significantly less than the substrate. On the Cr substrate, the wires show almost no contrast. Some wires appear slightly brighter than the substrate and some slightly darker. A strong dependence on the direction of the nanowire can also be seen, with nanowires lying in the plane of incidence (horizontally) being completely invisible, as indicated by the arrows in Fig. 2(d-e). The contrast, in this case, is topological and mainly due to a shadowing effect of the nanowire. The nanowires have diameters of 150–200 nm, which is well above the wavelength of the XUV radiation (∼40 nm). The increased brightness on the side facing the illumination can be explained by a mirror effect, where light reflected off the surface before the nanowire yields a higher XUV intensity at the side facing the illumination. The shadowing effect explains the dark side of the nanowires, and also why nanowires oriented parallel to the incoming radiation are not seen in the images (since the small shadow

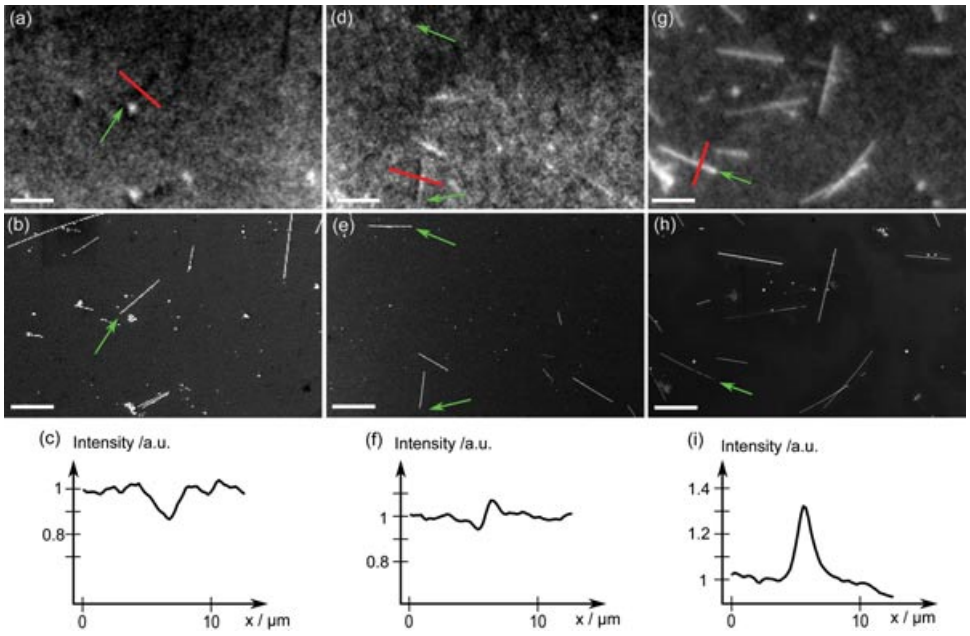

Figure 2 (online color at: www.ann-phys.org) PEEM images of Ag nanostructures on different substrates. The upper row shows images recorded using XUV attosecond pulse trains (400 s exposure times), the lower row shows reference images of the same areas recorded using SEM. Identical positions in the two images are indicated by the green arrows. The illumination is incident from the right in the XUV images. Bottom: Profiles measured along the indicated red lines in the XUV images. The substrates are ITO (a-c), Cr (d-f) and Au (g-i) All scale bars are 10 μm. Our resolution limit with the XUV pulses is $\sim$ 200 nm, which was measured using a lithographically defined structure.

at the short end of the nanowire cannot be resolved in the images).

Finally – on the Au substrate, the Ag nanowires appear significantly brighter than the substrate, giving a clear contrast. One can also see that vertical nanowires have one brighter and one darker side, while horizontal wires show a more homogeneous bright intensity distribution. The bright contrast is due to electronic structure differences, while the dark part is a topological shadowing effect. Even with a broadband light source and no energy filtering, good imaging conditions using SEs can be obtained for samples that are relevant for plasmonic studies. From profiles across wires as seen in the bottom row of Fig. 2, we find that the nanowires are up to 30% brighter than the Au substrate, while the contrast on the Cr substrate is below 10%, both for the bright side and the dark side of the wire. On the ITO substrate, the wires are $\sim$15% darker than the substrate. These contrast differences must come from the SEs, since they constitute more than 90% of the total electron yield. Differences in SE emission can be explained by differences in absolute work function between the different materials, or differences in excitation probabilities of either primary or secondary electrons. Au has been reported to have a higher workfunction than Ag (5.1 eV for Au and 4.1–4.7 eV for Ag) which would explain the contrast difference in that case. For both ITO and Cr lower work functions than for Au have been reported.

To investigate the plasmonic response of our sample in the current experimental setup, the fundamental of the laser beam was used to map out localized field enhancements on the sample. The Mach-Zehnder interferometer of our setup (see Fig. 1) gives us an excellent IR-pump – IR-probe setup by closing the gas bottle used for HHG and removing the Al filter. IR-pump – IR-probe investigations are highly complementary to IR-XUV experiments, as they visualize the localized plasmonic field in the surface region of the particle in a non-linear (and thus very sensitive) fashion [9–13]. Figure 3(a) shows overlaid PEEM images of Ag nanowires on Au acquired using a Hg lamp (greyscale), p-IR radiation (blue) and s-IR (red), respectively. For the p-polarization, the electric field is in the plane of incidence, while for the s-polarization the electric field lies in the sample plane. The localized hot spots and the large difference between the two orthogonal polarizations are typical signs of localized surface plasmons enhancing the near-field. While field enhancement in nanostructures can have several causes [39], plasmon resonances are usually observed for Ag nanostructures

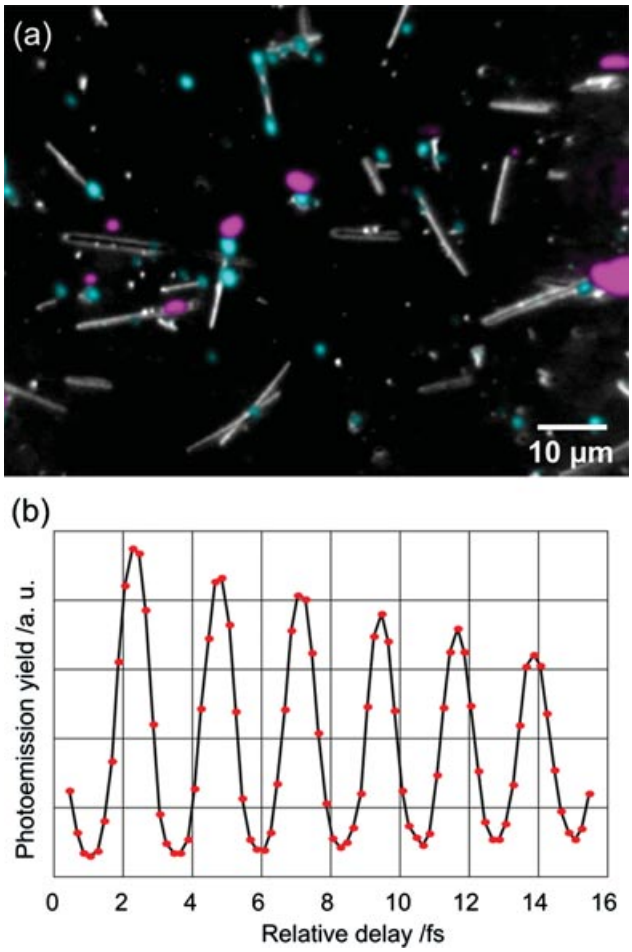

Figure 3 (online color at: www.ann-phys.org) (a) Overlaid PEEM images of Ag nanowires on Au, recorded using Hg lamp (greyscale), p-polarized IR light (blue) and s-polarized IR light (red). The Hg lamp excitation just above the workfunction threshold results in a depiction of the position and shape of the nanowires convoluted with any workfunction differences. The laser light is incident from the right side in the figure. (b) Measured intensity from hot-spots as a function of relative delay between two s-polarized IR pulses.

illuminated by visible or near-IR radiation. Similar behaviour is found on all three substrates indicating that it is indeed coupled to the Ag nanostructures. We observe that both Ag nanowire intersections, end-sections and a variety of Ag particles give rise to resonant enhancement. Our results agree with previous PEEM studies using two-photon photoemission [9–13] or higher-order photoemission [14–16].

We investigated the temporal stability of our pump-probe PEEM setup by measuring the photoemission intensity from single hot-spots as a function of delay between the two IR pulses in steps of 200 as. The correlation trace could be mapped out with sub-cycle precision, as seen in Fig. 3(b). Scanning the whole range from -60 fs to $+60$ fs with sub-cycle precision, we saw no significant difference in the widths or phases of the correlation traces, indicating that the plasmon lifetimes are either similar for different hot spots or, more likely, significantly shorter than the total IR pulse length of 35 fs. When changing the polarization of one of the beams, interference effects could still be observed despite orthogonal polarizations of the incoming beams. This confirms the near-field character of our probe method, since s- and p-polarizations are not properly defined in the near-field [40].

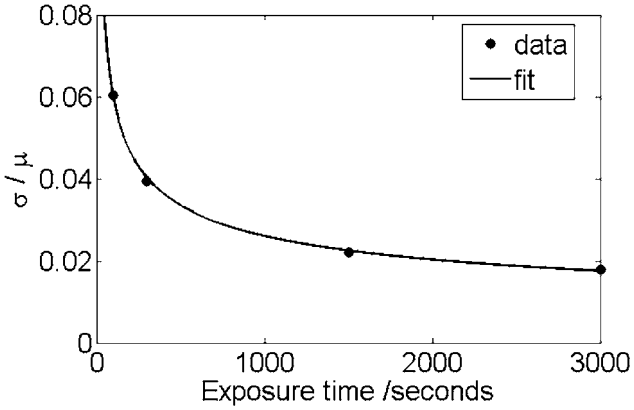

Figure 4 Noise ratio for different exposure times as derived from our experimental measurements. For a featureless area of the substrate, the standard deviation σ normalized by the mean value μ is measured. The data points are well fitted by a power law with an exponent of -0.4.

An interesting observation from comparing the XUV and IR excitation of the plasmonic samples is the quantitative evaluation of the relative strength between the multi-photon photoemission signal and the XUV signal. When combining an IR beam with a peak intensity of about 10^{13}–10^{14} W m^{-2} with the APT in our setup, we conclude that even in the hot spots, most of the detected photoelectrons come from the XUV. Having established conditions for achieving good contrast, we investigated if small oscillations in the XUV signal (a 10% peak-to-peak sine oscillation of imaged electrons) can be observed with our experimental system with reasonable exposure times. The main source of noise is the counting statistics of the SEs hitting the channelplate, which does not completely follow a simple Poisson distribution [41]. We have measured the noise in our images (the standard deviation σ normalized by the mean value μ) as a function of exposure time, as shown in Fig. 4. This corresponds to the noise in one pixel (of the channelplate). For comparison, a constant signal overlaid with a sine wave

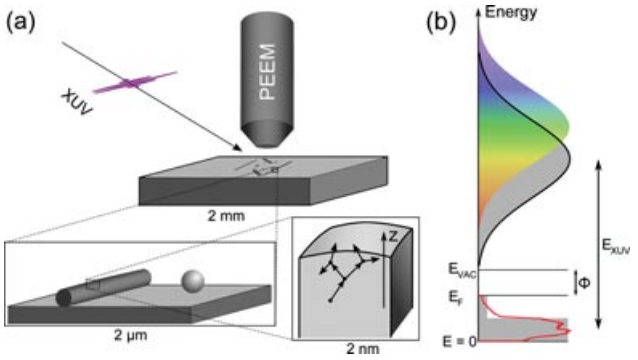

Figure 5 (online color at: www.ann-phys.org) (a) Schematic model of the SE emission. The volume of the SE cascade which is imaged in the PEEM is typically a few nanometers. (b) Energy diagram showing the important quantities in our model of the SE cascade. In the bottom, the measured density of states (DOS) of Ag is shown as a red line, together with our approximation (grey shaded area). The multi-coloured distribution shows the spectrum of an attosecond pulse with central energy 30 eV and FWHM 15 eV. The grey area corresponds to the distribution of primary electron energies in our model, and is a convolution between the XUV spectrum and the Ag DOS. In fact, due to the broad distribution of the XUV radiation, the convolution of the XUV with the approximate DOS is practically indistinguishable from that with the measured DOS.

with 10% peak-to-peak modulation would give value of $\frac{\sigma}{\mu} = \frac{1}{20\sqrt{2}} \approx 0.035$. From Fig. 4, we can therefore conclude that one should be able to statistically pick out a ∼10% oscillating signal in a single pixel with exposures of 500 s or more. Thus we end up with realistic time series of the order of a few hours for mapping out a significant time window.

3 Simulation of the SE cascade from a single attosecond XUV pulse

Finally, we present a model calculation of the time scale of a SE cascade for our experimental conditions, i.e. PEEM imaging and excitation by a ∼30 eV XUV attosecond pulse of a Ag surface – as sketched in Fig. 5(a). The single XUV attosecond pulse hits the sample, generating primary electrons, which then scatter with other electrons inside the material leading to a cascade of SEs. Two reasons for possibly observing a rather fast release of the SE cascade in this particular PEEM experiment is that the SEs with energies less that the work function threshold (3–5 eV) will not be imaged (as they do not leave the surface) and that the photo excitation energies are only ∼30 eV – much lower than in ordinary electron microscopes or at synchrotron sources.

We calculate how the SE cascade originating from an attosecond XUV pulse evolves with time through a semiclassical Monte Carlo simulation, based upon established models for SE generation [42–44], also used by Baggesen & Madsen [45] for application to attosecond spectroscopy from surfaces. Semiclassical models of electron propagation have been shown to capture the relevant physics and often give reliable quantitative results in areas such as attosecond physics [46, 47], solid state physics [43, 44], and secondary electron emission [45]. An example of an SE cascade is shown schematically in Fig. 5(a). We consider an SE cascade in a small volume near the surface of the metal and perform a one-dimensional simulation. This assumption holds as the electron mean free path is much shorter than the typical dimensions of the nanostructure. The approximations made in this model of an abrupt potential step at the surface are confirmed by theoretical studies showing that the potential step at noble metal surfaces effectively occurs within a few Ångström [48,49]. This is significantly smaller than the dimensions of the SE cascade. The other main components in the model are as follows: the electrons in the metal are treated as free particles with kinetic energy $E = \mathbf{p}^2/2m$, where m is the free electron mass and energies correspond to the bottom of the conduction band. The simulation starts with an electron being created at a random position within the outermost 5 nm of the metal at time $t = 0$ with a kinetic energy drawn from a distribution which is a convolution between the Gaussian profile of the attosecond pulse and an approximate density of states (DOS) for the filled 4d and 5s states of Ag, as indicated in Fig. 5(b). This density of states is an approximation of calculated and measured band structures of Ag, such as those published by Hüfner *et al.* [50] or calculated using the script of Ortiz *et al.* [51]. The electron is allowed to propagate for a lifetime τ drawn from an exponential distribution with mean value $\tau_0 = \alpha(E - E_F)^{-2}$, where $\alpha = 38$ fs eV^2. The value of this constant varies somewhat throughout literature, with reported values for Ag between 10 and 40 fs eV^2. [52–56] The lower value has been reported using several different experimental and theoretical approaches and seems most trustworthy, however we still use the larger value to not underestimate the time scale for the SE cascade. At the relevant energies, the scattering can be assumed to be spherically symmetric and the amount of energy lost by the electron roughly follows a rectangular distribution [42]. The electron (with kinetic energy E) in our model thus excites a new electron from an energy level E_1 drawn from the DOS distribution. The electron transfers an energy ΔE, so that two new electrons with energies E-ΔE and E_1+ΔE are created, where both of the new electrons must have

energies above the Fermi level. Electrons with energies below the vacuum level are discarded since they cannot escape from the surface, but electrons with energy above the vacuum level are given a new random direction and are allowed to propagate until the next scattering event. If an electron reaches the surface, it can escape if it has enough momentum normal to the surface, i.e. if $p_z > \sqrt{2m(E_F + \phi}$.) Otherwise, the electron is reflected, i.e. $p_z \rightarrow -p_z$.

We tested the validity of this model by changing the input parameters to a monochromatic excitation source and compared the spectrum to an XPS spectrum recorded from a Ag(111) single crystal at beamline I311 at MAX-lab. The model is in good qualitative agreement with the experimental spectra, as seen in Fig. 6(a). The excitation depth of 5 nm assumed in our calculation was chosen after careful evaluation of the scattering of electrons with an energy distribution as induced by the XUV pulse. Increasing the depth further did not lead to any significant increase in the number of emitted secondary electrons. This can be understood in that we image only the SEs that has a high enough kinetic energy to overcome the work function barrier. Thus secondary electrons with lower energies might travel longer in the material, but they are never observed in our PEEM.

The main result, of our model calculation, is seen in Fig. 6(b), showing the intensity of secondary electrons released as a function of time from the original XUV pulse excitation of primary electrons. Average lifetimes of approximately 1.9 fs for electrons at the vacuum level and 180 as for electrons 10 eV above the vacuum level mean that the SE cascade takes place within a fraction of an optical cycle of an IR beam with wavelength of 800 nm. In fact, 80% of all electrons are released within the first femtosecond. The extremely fast emission of the secondary electrons can be understood by observing that the electrons on average only undergo 2–3 scattering events before their energies are reduced to below the work function threshold (and are thus never emitted from the surface). The electrons need to cross the work function barrier to be imaged by the PEEM, thus while the final part of the SE cascade (with electrons of energy smaller than the work function energy) will happen over much longer times and occupy a larger part of the material, these SEs are not visible in the PEEM experiment which only observes the photoemitted electrons. Our model also gives indications of the spatial extent of the SE cascade in the model. This can be estimated by modifying the Monte Carlo simulation to keep track of 3D coordinates of each electron and monitor the escape positions. We note that more than 80% of the electrons emitted from a point at the surface originate from a primary electron excitation less than 1 nm away laterally, and less than 2 nm into the metal.

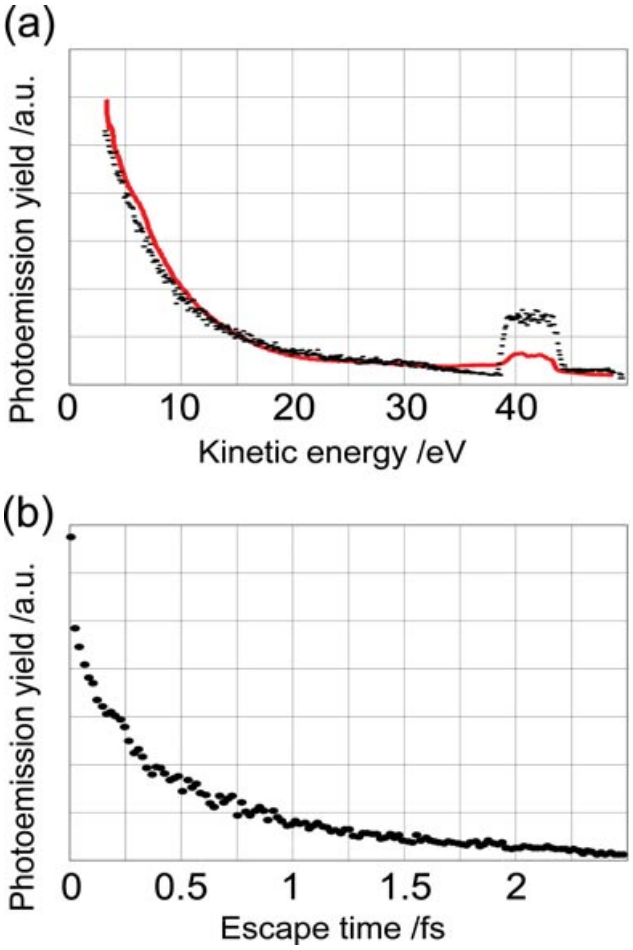

Figure 6 (online color at: www.ann-phys.org) (a) Calculated spectrum of photoemitted electrons following excitation by a monochromatic XUV source with an energy of 43 eV. The black dots correspond to our Monte Carlo simulation and the red line to experimental XPS spectra of a Ag(111) surface measured with 43 eV photons. (b) Total calculated photoemission yield as a function of time for the first 2.5 fs after initial XUV excitation.

4 Conclusions

Experimentally we investigated imaging of nanoplasmonic structures using attosecond XUV pulse trains and IR fs pulses, working towards realizing this type of attosecond nanoplasmonic imaging. We studied the contrast of plasmonic Ag nanostructures in PEEM images recorded using XUV APTs. Ag nanostructures were found to be very difficult to image when deposited on Cr or ITO substrates, while Au substrate gave a very good

contrast. In IR-pump – IR-probe experiments with subcycle precision over >100 fs we showed the autocorrelation trace in 3-photon photoemission microscopy. The question is what is further needed to experimentally observe nanoscale plasmonic imaging with attosecond time resolution. A prerequisite is probably the use of SAPs together with short IR pulses and significant stability of the setup to allow imaging with exposures in the ∼500 s range. While two- and multiphoton PEEM both rely on nonlinear processes, which enhance the signal, performing IR-pump – XUV-probe experiments could mean measuring a weaker modulation. Still, we found that with exposure times per image of ∼500 s even very weak modulations in the observed signals could potentially be observed. Finally, theoretical calculations indicated that the part of the SE cascade imaged by the PEEM can be very fast, with 90% of all electrons emitted within half an optical cycle of the 800 nm IR field typically used to generate the XUV attosecond pulses.

Acknowledgements. We acknowledge Lars Bojer Madsen for fruitful discussions. This work was supported by the Swedish Research Council (VR), the Swedish Foundation for Strategic Research (SSF), the Crafoord Foundation, the Knut and Alice Wallenberg Foundation, the Marie Curie Intra-European fellowship ATTOCO, the European Research Council (ERC) advanced grant ALMA and startup grant ElectronOpera.

Key words. PEEM, attosecond, nanostructure, PhotoEmission, microscopy, XUV, IR.

References

[1] F. Krausz and M. Ivanov, Rev. Mod. Phys. **81**, 163–234 (2009).
[2] S. Maier, Nature Phys. **3**, 301–303 (2007).
[3] J. A. Schuller, E. S. Barnard, W. Cai, Y. C. Jun, J. S. White, and M. L. Brongersma, Nature Mater. **9**, 193–204 (2010).
[4] E. Ozbay, Science **311**, 189–193 (2006).
[5] D. K. Gramotnev and S. I. Bozhevolnyi, Nature Photon. **4**, 83–91 (2010).
[6] M. I. Stockman, S. V. Faleev, and D. J. Bergman, Phys. Rev. Lett. **87**, 167401 (2001).
[7] M. Pelton, J. Aizpurua, and G. Bryant, Laser & Photon. Rev. **2**, 136–159 (2008).
[8] J. Pitarke, V. M. Silkin, E. V. Chulkov, and P. M. Echenique, Rep. Prog. Phys. **70**, 1–54 (2007).
[9] M. Aeschlimann et al., Nature **446**, 301–304 (2007).
[10] L. I. Chelaru, M. Horn-von Hoegen, D. Thien, and F.-J. Meyer zu Heringdorf, Phys. Rev. B **73**, 115416 (2006).
[11] M. Cinchetti, A. Gloskovskii, S. A. Nepjiko, G. Schönhense, H. Rochholz, and M. Kreiter, Phys. Rev. Lett. **95**, 047601 (2005).
[12] G. H. Fecher, O. Schmidt, Y. Hwu, and G. Schönhense, J. Electron Spectrosc. Relat. Phenom. **126**, 77–87 (2002).
[13] A. Kubo, K. Onda, H. Petek, Z. Sun, Y. S. Jung, and H. K. Kim, Nano Lett. **5**, 1123–1127 (2005).
[14] L. Douillard et al., Nano Lett. **8**, 935–940 (2008).
[15] F. Schertz, M. Schmelzeisen, R. Mohammadi, M. Kreiter, H.-J. Elmers, and G. Schönhense, Nano Lett. **12**, 1885–1890 (2012).
[16] M. Aeschlimann, et al. Science **333**, 1723–1726 (2011).
[17] A. Liebsch, Electronic Excitations at Metal Surfaces. Plenum, New York (1997).
[18] P. J. Feibelman, Phys. Rev. B **12**, 1319–1336 (1975).
[19] N. J. Halas, S. Lal, W-S. Chang, S. Link, and P. Nordlander, Chem. Rev. **111**, 3913–3961 (2011).
[20] M. I. Stockman, M. F. Kling, U. Kleineberg, and F. Krausz, Nature Photon. **1**, 539–544 (2007).
[21] A. Mikkelsen et al., Rev. Sci. Instrum. **80**, 123703 (2009).
[22] S. H. Chew et al., Appl. Phys. Lett. **100**, 051904 (2012).
[23] A. Pietzsch et al., New J. Phys. **10**, 033004 (2008).
[24] M. Hjort et al., Appl. Phys. Lett. **99**, 233113 (2011).
[25] M. Hjort et al., ACS Nano **6**, 9679–9689 (2012)
[26] A. Howie, J. Microsc. **180**, 192–203 (1995).
[27] J. Stöhr et al., Science **259**, 658 (1993)
[28] Y. R. Fang, H. Wei, F. Hao, P. Nordlander, and H. X. Xu, Nano Lett. **9**, 2049–2053 (2009).
[29] H. Wei et al., Nano Lett. **11**, 471–475 (2011).
[30] E. C. Garnet et al., Nature Mater. **11**, 241–249 (2011).
[31] Y. G. Sun and Y. N. Xia, Adv. Mater. **14**, 833–837 (2002).
[32] H. Y. Liang, H. X. Yang, W. Z. Wang, J. Q. Li, and H. X. Xu, J. Am. Chem. Soc. **131**, 6068–6069 (2009).
[33] H. Wei, A. Reyes-Coronado, P. Nordlander, J. Aizpurua, and H. X. Xu, ACS Nano **4**, 2649 (2010).
[34] T. Fordell, M. Miranda, A. Persson, and A. L'Huillier, Opt. Express **17**, 21094 (2009).
[35] D. Guénot et al., Phys. Rev. A **85**, 053424 (2012).
[36] P. M. Paul et al., Science **292**, 1689–1692 (2001).
[37] H. G. Muller, Appl. Phys. B **74**, S17–21 (2002).
[38] R. López-Martens et al., Phys. Rev. Lett. **94**, 033001 (2005).
[39] L. Cao, J. S. White, J-S. Park, J. A. Schuller, B. M. Clemens, and M. L. Brongersma, Nature Mater. **8**, 643–647 (2009).
[40] H.W. Kihm et al., Nature Commun. **2**, 451 (2011).
[41] L. Frank, J. Electron Microsc. **54**, 361–365 (2005).
[42] P. A. Wolff, Phys. Rev. **95**, 56–66 (1954).
[43] A. Dubus et al., Phys. Rev. B **47**, 11056–11073 (1993).
[44] T. Koshikawa and R. Shimizu, J. Phys D **7**, 1303–1315 (1974).
[45] J. C. Baggesen and L. B. Madsen, Phys. Rev. A **80**, 030901 (2009).
[46] P. B. Corkum, Phys. Rev. Lett. **71**, 1994–1997 (1993).
[47] M. Lewenstein, Ph. Balcou, M. Yu. Ivanov, A. L'Huillier, and P. B. Corkum, Phys. Rev. A **49**, 2117–2132 (1994).
[48] N. D. Lang and W. Kohn, Phys. Rev. B **3**, 1215–1223 (1971).

[49] P. C. Rusu, G. Giovannetti, C. Weijtens, R. Coehoorn, and G. Brocks, Phys. Rev. B **81**, 125403 (2010).
[50] S. Hüfner, G. K. Wertheim, N. V. Smith, and M. M. Traum, Solid State Commun. **11**, 323–326 (1972).
[51] C. Ortiz, O. Eriksson, and M. Klintenberg, Comput. Mater. Sci. **44**, 1042–1049 (2009).
[52] E. Knoesel, A. Hotzel, T. Hertel, M. Wolf, and G. Ertl, Surf. Sci. **368**, 76–81 (1996).
[53] F. Weik, A. de Meijere, and E. Hasselbrink, J. Chem. Phys. **99**, 682–694 (1993).
[54] H. Petek and S. Ogawa, Prog. Surf. Sci. **56**, 239–310 (1997).
[55] L. Burgi, O. Jeandupeux, H. Brune, and K. Kern, Phys. Rev. Lett. **82**, 4516 (1999).
[56] A. Garcà-Lekue et al., Phys. Rev. B **68**, 045103 (2003).